Published in final edited form as:
Immunity. 2009 March 20; 30(3): 408–420. doi:10.1016/j.immuni.2009.01.010.

The lymphotoxin $LT\alpha_1\beta_2$ controls postnatal and adult spleen marginal sinus vascular structure and function

Carlene L. Zindl[1,2], **Tea Hyun Kim**[2], **Meiqin Zeng**[2], **Angela S. Archambault**[1], **Mitchell H. Grayson**[3,4], **Kyunghee Choi**[1], **Robert D. Schreiber**[1], and **David D. Chaplin**[2,5]

[1]Department of Pathology and Immunology, Washington University School of Medicine, St. Louis, MO 63110, USA

[2]Department of Microbiology, University of Alabama at Birmingham, Birmingham, AL 35294, USA

[3]Department of Medicine, Division of Allergy and Immunology, Washington University School of Medicine, St. Louis, MO 63110, USA

Summary

The lymphotoxin $LT\alpha_1\beta_2$ supports the development and maintenance of several aspects of spleen structure, but its significance for marginal sinus (MS) vascular organization is unclear. We showed here that in early postnatal lymphotoxin-deficient mice, the developing Flk-1^+ white pulp vessels failed to organize or up-regulate MAdCAM-1, leading to altered spatial rearrangement of both the white pulp endothelial cells and the smooth muscle actin expressing cells. *In vitro*, MAdCAM-1 directed the reorganization of LTβ receptor$^+$ endothelial cells grown on Matrigel. $LT\alpha_1\beta_2$ also regulated the maintenance of both MAdCAM-1 expression and mature MS structure in adult mice, contributing importantly to normal trafficking of $CD11b^+$ cells in response to bacterial antigens. Together our studies demonstrate that $LT\alpha_1\beta_2$ and LTβ receptor signals control proper development and maintenance of the mature MS structure and implicate MAdCAM-1 in the structuring of the MS endothelial cells that is important for the movement of immune cells within the spleen.

Keywords

MAdCAM-1; Flk-1; lymphoid organ; development; cytokine

Introduction

The spleen is a secondary lymphoid tissue with an important role in host defense against blood-borne pathogens, particularly encapsulated bacteria (Bohnsack and Brown, 1986; Ejstrud et al., 2000; Waghorn, 2001). Cells and particles enter the spleen through the marginal sinus (MS) and then continue to the marginal zone (MZ) area which contains several types of resident immune cells (i.e. macrophages, MZ B cells, dendritic cells) that 'sample' the blood for foreign antigens (Kraal, 1992; Kraal and Mebius, 2006; Mebius and Kraal, 2005; Mebius et al., 2004).

Scanning electron microscopy (SEM) of micro-corrosion casts of mouse spleen show that the MS consists of a flattened, interconnecting vascular network originating from multiple tubular vessels that branch off the central arterioles (Schmidt et al., 1985). The nature of the

[5]Correspondence: dchaplin@uab.edu, Phone: 205-934-9339, Fax: 205-934-9256.
[4]Current affiliation: Department of Pediatrics, Division of Allergy and Clinical Immunology, Medical College of Wisconsin, Milwaukee, WI 53226, USA

endothelium lining the MS is unclear, but the MS endothelial cells express both ephrinB2, a marker that in other anatomical sites is restricted to arterial vessels (Gale et al., 2001; Kraal et al., 1995; Shin et al., 2001; Wang et al., 1998) and the adhesion molecule MAdCAM-1 (Kraal et al., 1995).

The functional significance of MAdCAM-1 in the spleen is unknown. Systemic blockade with MAdCAM-1 antibodies does not appear to alter cell trafficking to the spleen under conditions that halt trafficking of lymphocytes to mucosal secondary lymphoid tissues (Kraal et al., 1995). In sphingosine-1-phosphate (S1P) lysophospholipid receptor $S1P_3$-deficient mice which have abnormally distributed splenic MS expression of MAdCAM-1 (Girkontaite et al., 2004), the MZ B cells enter the white pulp (WP) nodules faster in response to LPS than in wild type (WT) mice. These data suggest that MAdCAM-1 organization may contribute to proper trafficking of cells from the MZ to the white pulp.

Proteins of the lymphotoxin (LT) and TNF family play key roles in establishing secondary lymphoid tissue organization. $LT\alpha_1\beta_2$ and the LTβ receptor (LTβR) deliver essential signals *in utero* for lymph node and Peyer's patch organogenesis (Rennert et al., 1996; Rennert et al., 1998). LTβR-Ig transgenic mice and mice treated passively with the LTβR-Fc indicate that interactions between $LT\alpha_1\beta_2$ and the LTβR after E17 and during neonatal development are important for establishing proper splenic architecture (Ettinger et al., 1996; Mackay et al., 1997; Rennert et al., 1996). The spleens of adult $Lta^{-/-}$, $Ltb^{-/-}$, and $Ltbr^{-/-}$ mice show absence of follicular dendritic cell (FDC) clusters, failure to segregate T and B cells into discrete zones, absence of MZ cells, and loss of MAdCAM-1 on the sinus-lining cells (Banks et al., 1995; De Togni et al., 1994; Fu and Chaplin, 1999; Futterer et al., 1998; Koni et al., 1997).

$Tnf^{-/-}$ and $Tnfrsf1a^{-/-}$ (*TNFRI-deficient*) mice have lymph nodes, but show defects in spleen architecture (Neumann et al., 1996; Pasparakis et al., 1996; Pasparakis et al., 1997). In these mutant mice, WP B cells form abnormal 'ring-like' structures, FDCs are abnormally localized in the MZ (Pasparakis et al., 2000), and the numbers of macrophages in the MZ are reduced.

Mice deficient in several transcription factors of the NF-κB family also manifest defective spleen organization. Recently, mice doubly deficient in the p50 and p52 NF-κB subunits or mice deficient in RelB have shown abnormal formation of MZ and germinal center (GC) structures similar to $Ltbr^{-/-}$ mice (Lo et al., 2006; Weih et al., 2001). In addition, MZ structures and B cell areas appear absent in alymphoplastic *aly/aly* mice which carry a spontaneous point mutation in the gene encoding NF-κB-inducing kinase (NIK) (Koike et al., 1996). $Map3k14^{-/-}$ mice (NIK-deficient) also display abnormalities in lymph node organogenesis and splenic architecture similar to those seen in *aly/aly* and $Ltbr^{-/-}$ mice (Yin et al., 2001). Importantly, NIK regulates the transcriptional activity of the NF-κB complex via the alternative pathway specifically in response to LTβR stimulation (Dejardin et al., 2002; Matsushima et al., 2001; Smith et al., 2001; Yin et al., 2001).

Although overall spleen architecture is dramatically disturbed in $Lta^{-/-}$ and $Ltbr^{-/-}$ mice, studies of MS structure have been hindered by a lack of appropriate cell surface markers because $LT\alpha_1\beta_2$ is required for MAdCAM-1 expression. Here, we identified additional markers that permit specific detection of WP vascular structures in both WT and LT and TNF family deficient mice. Immunostaining of thick spleen sections and imaging of neonatal mice using confocal microscopy demonstrate that, during the first week after birth, sinus endothelial cells failed to up-regulate MAdCAM-1 and failed to organize normally at the edge of the developing WP structures of $Lta^{-/-}$ and $Ltbr^{-/-}$ mice. These data implicate $LT\alpha_1\beta_2$–dependent signals as critical for the formation of mature marginal sinus vascular structure. *In vitro*, $LT\beta R^+$ endothelial cells can utilize MAdCAM-1 to reorganize, indicating that MAdCAM-1 may contribute to the normal MS organization of the developing spleen endothelial cells in the

postnatal period. Furthermore, structural analyses reveal that continuous LTβR signals were required to maintain normal MAdCAM-1$^+$ MS organization in adult mice, an organization that importantly supports the movement of local immune cells responding to microbial challenge.

Results

Flk-1 is expressed on murine spleen marginal sinus endothelial cells

By investigating antigens that may mark MS cells in an LT-independent fashion, we found that Flk-1 (VEGFR-2) was predominantly expressed in the MS area and on vessels more centrally located within the WP (Figure 1A). Weak Flk-1 staining could also be detected on the sinusoidal structures in the red pulp (RP). VE-cadherin (CD144), similar to PECAM-1 (CD31), was expressed on vascular endothelial cells in both the WP and RP. Interestingly, VE-cadherin staining was reproducibly weaker on MS vessels compared to the high expression seen on RP vessels (Figure 1B).

Because macrophages can express low amounts of Flk-1, we compared by confocal microscopy the pattern of expression of Flk-1 with that of PECAM-1 and MOMA-1 which recognizes the metallophilic macrophage cells that are located closest to the MS structure (Kraal and Janse, 1986). Flk-1 co-localized with PECAM-1 (Figure 1C) and not with MOMA-1 (Figure 1D), demonstrating that the Flk-1 antibody specifically recognized endothelial cells in the MS. Most of the MOMA-1$^+$ metallophilic macrophages were located peripheral to the MS in the MZ, with few MOMA-1$^+$ cells found within the WP areas of naïve mice.

SMA$^+$ cell organization identifies distinct vessels within the white pulp

MZ-associated smooth muscle actin (SMA)$^+$ cells have been documented in rodents and primates (Steiniger and Barth, 2000). Because ephrinB2 is selectively expressed on the ‘arterial’ vasculature of the spleen WP including vessels in the MS area (Gale et al., 2001; Shin et al., 2001), we questioned whether smooth muscle cells were also associated with the MS. SMA staining in mouse spleen was mostly restricted to the WP areas, with the exception of the large vessels in the RP (Figures 1E, 1F). Strong SMA staining was observed around the WP central arterioles. Interestingly, in 20μm sections of spleen, SMA$^+$ cells were also detected within the T cell areas and at the MS border.

In order to analyze the distribution patterns of the smooth muscle and endothelial cells within the WP and at the MS border in greater detail, we used confocal microscopy and compiled multiple images to construct a 6 μm thick section (Figure 1G). Using this approach, it was apparent that the central arteriole and the arterial branching vessels showed the strongest SMA staining. SMA staining near the MS network appeared to be present as fibrils localized primarily on the WP side (Figure 1H). These data show that SMA$^+$ cells form a platform under rather than encasing the MS vessels as they do the central arteriole and arterial branching vessels.

LTβR signaling is required for normal marginal sinus structure

The structure of the MS has not been well characterized in the spleens of adult *Lta*$^{-/-}$ and *Ltbr*$^{-/-}$ mice because these mice lack expression of MAdCAM-1. Staining 20 μm thick spleen sections with the Flk-1 and SMA antibodies indicated that Flk-1$^+$ VE-cadherin$^+$ endothelial cells were present but did not form a normal MS structure in *Lta*$^{-/-}$ or *Ltbr*$^{-/-}$ mice (Figure 2A). Balogh and colleagues also observed disturbed MS structure in *Ltbr*$^{-/-}$ mice using the rat antibody, IBL-7/1, which recognized MS structures in WT mice (Balazs et al., 2001; Balogh et al., 2007). However, we observed a few Flk-1$^+$ VE-cadherin$^+$ endothelial cells scattered around the borders of the WP areas in targeted animals (see enlarged images). Serial 20 μm thick sections of spleens of *Lta*$^{-/-}$ and *Ltbr*$^{-/-}$ mice showed SMA$^+$ cells associated with the

scattered Flk-1$^+$ cells localized at the border of the WP nodules. This suggested that some vascular component with features consistent with a MS structure might be present. The organization of the SMA$^+$ smooth muscle cells within the WP was also abnormal in *Lta*$^{-/-}$ and *Ltbr*$^{-/-}$ mice (Figure 2B), with a larger number of SMA$^+$ cells localized around the central arteriole structures. This phenotype demonstrated that LTβR signaling affected the distribution of both endothelial cells and smooth muscle cells within the WP.

Interestingly, *Tnfrsf1a*$^{-/-}$ mice showed a nearly normal MS structure with some regional discontinuity in the vascular network around the WP nodules (Figure 2A). Thus, TNFRI signals are not required for the presence of a MS vascular border but may contribute to the complete maturation of these vessels.

To further assay the importance of LTβR signaling, we analyzed the MS architecture in *Map3k14*$^{-/-}$ mice. In the spleens of *Map3k14*$^{-/-}$ mice, SMA$^+$ cells showed displacement similar to that seen in *Ltbr*$^{-/-}$ mice and showed no recognizable MS vascular structure and no Flk-1$^+$ cells at the borders of the WP nodules (Figure 2B). The few vascular structures that could be identified were found primarily in the centers of the WP (representing central arterioles) and in the RP areas. These data implicate NIK in the signaling that controls endothelial cell and smooth muscle cell localization in the MS, but also suggest that NIK participates in signaling events mediated by other receptors in addition to the LTβR.

To test whether the few scattered Flk-1$^+$ cells that could be detected at the borders of the WP nodules in *Lta*$^{-/-}$ mice (Figure 2) were part of the WP or the RP vessels, we compared the expression of ephrinB2 in WT and *Lta*$^{-/-}$ mice. In WT mice ephrinB2 is specifically expressed on the WP 'arterial' vessels and also on the MS vasculature (Figure 3A) (Gale et al., 2001;Shin et al., 2001). Interestingly, 10μm thick spleen sections from *Efnb2*$^{+/-}$ *Lta*$^{-/-}$ mice also show scattered ephrinB2$^+$ cells at the borders of the WP nodules in a pattern similar to Flk-1 (Figures 2A and 3B). This suggests that these peripheral endothelial cells in *Lta*$^{-/-}$ mice are analogous to the MS endothelial cells of WT animals.

In order to obtain a more detailed picture of the three-dimensional organization of the MS endothelial cells, we cut 120 μm spleen sections using a sliding microtome, compiled image stacks, and compared the MS area of part of a WP nodule in *Efnb2*$^{+/-}$ *Lta*$^{+/+}$ and *Efnb2*$^{+/-}$ *Lta*$^{-/-}$ mice (Figures 3C and 3D). The cytoplasmic localization of β-galactosidase activity in ephrinB2$^{+/-}$ knock-in mice allowed increased signal to noise ratio for confocal imaging of thick spleen sections; however, similar results were obtained using the Flk-1 antibody (not shown). The branching arterial (BA) vessels in *Efnb2*$^{+/-}$ mice bifurcate repeatedly through several orders until they form the complex network of interconnecting vascular channels that constitute the MS (Figure 3C). In some areas (see rotating supplemental images: S1 and S2), the sinus endothelium appears flattened in a fashion similar to the structures observed in the SEM microcorrosion casts obtained by Schmidt (1985). Similar structural features have been shown using intravital microscopy (Grayson et al., 2001). Distinct gaps in the MS vasculature were detected, appearing well positioned to permit movement of cells between the central WP and the more peripheral MZ. These key features of the MS structure were all abnormal in *Efnb2*$^{+/-}$ *Lta*$^{-/-}$ mice (Figure 3D) with a loss of approximately 80% of the MS vascular region (Figure 3E). The MS ephrinB2$^+$ endothelial cells in the LTα-targeted animals have a thin, tubular shape similar to that of the branching arterial vessels and do not appear to have the extensive interconnections or flattened structures typical of the MS. Thus, LT$\alpha_1\beta_2$ and LTβR signals are crucial for the proper organization of the MS vascular structure.

LT$\alpha_1\beta_2$ dictates proper MS development during the first week of life

The absence of normally complex MS structures in adult *Lta*$^{-/-}$ (Figures 2 and 3) and *Ltbr*$^{-/-}$ mice (not shown) indicated that this signaling pathway is required for the development

of the MS. Balogh and colleagues using rat antibodies to mouse spleen antigens had observed that between birth and 1 week of age, distinct RP and WP areas formed and that the IBL-7/1 antigen became specifically localized at the developing sinus area, indicating that the early postnatal period was crucial for spleen vascular development (Balazs et al., 2001; Balogh et al., 2007). To determine when the MS endothelial and smooth muscle cells participate in the formation of a mature MS structure, we followed the appearance and distribution of these cells during early postnatal development of the spleen using the Flk-1 and SMA antibodies (Figure 4A). WT spleen on day 1 had vascular structures that could not yet be distinguished as specifically RP or WP anlagen (data not shown).

Development of discrete WP and RP vascular structures and influx of lymphocytes occurred rapidly after birth. By day 3, large numbers of $B220^+$ cells had entered the spleen. In addition, SMA^+ cells were found around centrally localized structures that are likely arborizing central arterioles. The majority of Flk-1^+ cells were found in the developing RP areas. At this same time, small numbers of Flk-1^+ cells started to congregate around the edge of the B cell clusters in the developing WP areas (Figure 4A).

Within the next 2 to 4 days, the pattern of expression of the SMA^+ and Flk-1^+ cells changed. The SMA^+ cells were more widely distributed within the WP areas. The Flk-1^+ cells were no longer concentrated in the RP areas but had come together to form a border around the clusters of B cells in the developing WP areas. At this time, the developing Flk-1^+ MS was still not a mature structure and B cells had not achieved a follicular organization. By 1 wk after birth, the developing MS of the spleen consisted of clusters of Flk-1^+ vessels (Figure S3).

By 2 wks after birth, the clusters of B cells and T cells had expanded to form discrete zones but most of the SMA^+ cells were not yet associated with the Flk-1^+ cells in the MS. In addition, the MS structure at this time was not as tightly organized as in the adult tissue. The distribution of the Flk-1^+ cells in the MS at 2 wks of age appeared less condensed than in the adult. By 3 wks of age, the MS structure was very similar to that seen in adult tissue (6 to 8 wks), with the Flk-1^+ cells forming a tight border associated with SMA^+ cells around the MS (data not shown) and numerous branching arterioles terminating at the MS (Figure S3).

Examination of the spleens of $Lta^{-/-}$ mice (Figure 4A) and $Ltbr^{-/-}$ mice (data not shown) during the first wks after birth showed defects in several of the developmental events described above. On day 5, smooth muscle cells in $Lta^{-/-}$ spleens showed no association with the WP and SMA staining could only be found around the central arterioles. By several criteria, $Lta^{-/-}$ spleens at day 5 resembled WT spleens at day 1, with the majority of the Flk-1^+ cells still found in the RP areas. By day 7, reorganization of the Flk-1^+ vessels at the periphery of the B cell zones remained impaired (Figure S3). By day 14, $Lta^{-/-}$ B cells still had not migrated away from the central arteriole structures and thus had not formed discrete B cell follicles. Also, SMA^+ cells were still not widely distributed and no distinct MS structures could be found. In adult $Lta^{-/-}$ spleens, the smooth muscle cells in the WP were largely distributed close to the central arteriole structures, and were sometimes found in contact with the few Flk-1^+ cells that separated B cells from the RP. Furthermore, at 3 wks, the spleens of $Lta^{-/-}$ mice had reduced numbers of branching arterial vessels and connecting sinus vessels compared to WT mice (Figure S3). Our analysis comparing development of the MS structure over the first few days after birth showed differences between WT and $Lta^{-/-}$ as early as day 3, suggesting that some of the critical aspects of LTβR signaling must be occurring at or prior to this time period.

$LT\alpha_1\beta_2$ up-regulation of MAdCAM-1 may participate in MS vascular organization

MAdCAM-1 regulates the homing of lymphocytes to neonatal lymph nodes (Mebius et al., 1996). To address whether MAdCAM-1 also contributed to the postnatal population of the splenic environment, we analyzed the expression and localization of MAdCAM-1 in the

developing neonatal spleen. MAdCAM-1 protein was detected in the spleen on postnatal days 3 and 5 in WT, *Tnfrsf1a*$^{-/-}$, *Lta*$^{-/-}$ and *Ltbr*$^{-/-}$ mice (Figures 4B and 4C); however, in *Lta*$^{-/-}$ and *Ltbr*$^{-/-}$ mice, MAdCAM-1 protein was significantly reduced in spleen at 1 and 2 wks of age. Interestingly, in the WT and mutant strains on day 3, MAdCAM-1 expression was localized to the RP vessels (Figure 4D). By day 5, MAdCAM-1 expression could be detected in the developing MS area of WT and *Tnfrsf1a*$^{-/-}$ mice but not of *Ltbr*$^{-/-}$ mice. On day 7, MAdCAM-1 expression in WT and *Tnfrsf1a*$^{-/-}$ mice was predominantly in the MS area, whereas residual MAdCAM-1 protein in *Ltbr*$^{-/-}$ mice was localized to the large draining vessels in the RP. *Tnfrsf1a*$^{-/-}$ mice had a similar distribution of MAdCAM-1 at the MS border compared to WT mice, but showed reduced expression. On day 14, MAdCAM-1 expression in *Tnfrsf1a*$^{-/-}$ mice was also reduced and appeared less contiguous compared to WT mice, suggesting that MS structures require TNFRI signals to assume the fully developed adult organization. In contrast, MAdCAM-1 protein expression at the MS border was completely lost in *Ltbr*$^{-/-}$ mice at all periods of neonatal development analyzed. Because total spleen cellularity was similar in WT and *Ltbr*$^{-/-}$ mice, these data suggest that LTβR-dependent neonatal expression of MAdCAM-1 at the developing MS contributes primarily to the rearrangement of the Flk-1^{+} endothelial cells and to the formation of a properly organized MS vasculature. Additionally, MS formation early in neonatal development proceeded independent of TNFRI, but signaling through this receptor appears to play an important role in completing MS maturation during the transition to adult life.

LTβR^{+} endothelial cells demonstrate MAdCAM-1-dependent reorganization

Because splenic vascular cells require LT signals for reorganization during development, we questioned whether endothelial cells may be receiving a direct signal via the LTβR. Interestingly, LTβR protein appeared to be expressed by stromal-type cells throughout the spleen and also localized on cells in the marginal sinus area (Figure 5A). Spleen cells isolated with anti-Flk-1 or anti-CD144 have an endothelial cell phenotype, shown by their ability to bind acetylated low-density lipoprotein (AcLDL; Figure 5B) and to form capillary-like structures on Matrigel (Figure 5C). These primary splenic endothelial cells (sECs) and the well-characterized mouse brain endothelial cell line, bEnd.3 expressed the LTβR protein and mRNA (Figures 5D and 5E). Interestingly, immunoblotting detected two differentially migrating LTβR molecules, with the smaller protein showing strong expression in the primary splenic endothelial cells.

To assess the role of LTβR signaling in these sECs, we stimulated the Flk-1^{+} cells isolated from WT or *Lta*$^{-/-}$ mice with either a control antibody or an agonist LTβR antibody. Unlike the sECs from WT mice, the cells isolated from *Lta*$^{-/-}$ mice formed fewer cellular clusters between the capillary-like structures when plated on Matrigel (Figure 5F; arrows). However, sECs from WT and *Lta*$^{-/-}$ mice stimulated with anti-LTβR reorganized to form larger areas densely populated with endothelial cells compared to control antibody treated cells.

To directly test the ability of MAdCAM-1 to participate in endothelial cell reorganization, we transfected bEnd.3 cells with a FLAG-tagged MAdCAM-1 expression vector in which the FLAG tag was placed after the cytoplasmic tail (pMAdCAM-1-FLAG). Using AMAXA nucleofector transfection, bEND.3 cells showed strong FLAG protein expression and properly localize MAdCAM-1 to the plasma membrane (Figure S4). Compared to a control vector pBAP-FLAG, bEND.3 cells transfected with pMAdCAM-1-FLAG showed dose-dependent reorganization such that the bEnd.3 cells interacted with the Matrigel over a larger surface area (Figures 5G and 5H). This was not the result of increased cellular proliferation because the DNA content from the pMAdCAM-1-FLAG transfected cultures was similar compared to control transfected cultures (data not shown). Immunostaining cross-sections of endothelial cells grown on Matrigel with anti-FLAG indicated that the bEND.3 cells transfected with

pMAdCAM-1-FLAG had a more flattened phenotype and had an increase in membrane-associated MAdCAM-1 contacting the Matrigel compared to control transfected cells (Figure 5I; see enlarged images). Together, these data implicate high MAdCAM-1 expression in the flattened morphology of the MS vasculature and underscore the key role of $LT\alpha_1\beta_2$ in up-regulating MAdCAM-1 and in specifying the mature MS vascular structure.

Ongoing LTβR signaling is required to maintain the adult marginal sinus network

Administration of LTβR-Fc but not TNFRI-Fc to adult mice demonstrated that continuous $LT\alpha_1\beta_2$ signals were required to maintain fully differentiated spleen architecture (Mackay et al., 1997); however, because MAdCAM-1 expression on the marginal sinus was lost in those studies, the organization of the marginal sinus vasculature could not be assessed. We found that treatment of adult WT mice with a single dose of LTβR-Fc caused structural changes with a loss of ~50% of the Flk-1^+ MS vascular region compared to human Ig treated mice (Figures 6A and 6B). This abnormal phenotype was fully established at 2 wks after injection of the LTβR-Fc and did not resolve until one month after injection. Analysis of 10 μm sections revealed that the Flk-1^+ endothelium of treated mice reverted to a less complex pattern, resembling the underdeveloped vascular structures observed in *Lta*$^{-/-}$ and *Ltbr*$^{-/-}$ mice. Analysis of thicker spleen sections indicated that in the absence of $LT\alpha_1\beta_2$ signals there were wider gaps in the MS structure compared to controls, suggesting that treatment with the LTβR-Fc caused a major restructuring of the normally flattened MS vessels (Figure S5). Thus, continuous $LT\alpha_1\beta_2$ signals were required to maintain the normal marginal sinus vascular structure.

LT-dependent MS maintenance in adult mice contributes to proper cell localization

Early in the response to thymus independent (TI) antigens, resident MZ cells and leukocytes that enter the spleen from the blood rapidly localize to the MS area (Balazs et al., 2002). To assess whether normal MS vascular structure is required for the response to TI antigens, we pretreated WT mice with LTβR-Fc to disrupt the MS network, then examined the localization of immune cells in response to i.v. injection of *Staphylococcus aureus* (*S. aureus*) bioparticle antigens. Three hrs after injection of the Ag, immune cells were clustered at the border between the B cell follicles and the MS of LTβR-Fc-treated mice (Figure 6C). The distribution pattern of these leukocytes was indistinguishable from the pattern in mice treated with control Ig; however, the numbers of recruited cells appeared modestly reduced. This indicated that the initial migration of immune cells into the MZ area was not profoundly altered by the disruption of the adult MS vasculature. Later in the response of control animals (12 and 24 hrs after injection of *S. aureus* bioparticles), the majority of CD11b$^+$ cells and other cells laden with the *S. aureus* antigen were found localized in the RP where macrophages play an important role in clearing antigens (Karlsson et al., 2003). Interestingly, at 12 hrs and 24 hrs after injection of the bioparticles, mice treated with LTβR-Fc showed abnormal localization of CD11b$^+$ cells in the WP (Figure 6 C , D). These data suggest that $LT\alpha_1\beta_2$ signals, in addition to controlling the MS organization, may also contribute to the trafficking of CD11b$^+$ cells between the red and white pulp spleen compartments.

To probe the nature of the signals responsible for this abnormal localization of CD11b$^+$ cells, we also analyzed the cell localization response of several gene targeted mouse strains to challenge with *S. aureus* bioparticle antigens (Figure S6A, B). In the spleens of control Ig-treated B-cell deficient (*Igh6*$^{-/-}$) mice, CD11b$^+$ cells are normally distributed in the RP. In *Igh6*$^{-/-}$ mice treated with LTβR-Fc, i.v. challenge with *S. aureus* bioparticles elicited an abnormal distribution of CD11b$^+$ cells similar to that seen in LTβR-Fc-treated, *S. aureus* bioparticle-challenged WT mice. Thus, B cells are not required for the LT-dependent localization of CD11b$^+$ cells. Similarly, ICAM-1, which shows strong expression on the MS endothelium, was also not required for either the normal *S. aureus* driven localization of

$CD11b^+$ cells at the periphery of the WP or for the redistribution of a portion of these cells into the center of the WP area. For this experiment, we used the mouse induced mutant model in which all isoforms of ICAM-1 were absent (*Icam1*^{null}) (Bullard et al., 2007).

Intravenous (i.v.) challenge with *S. aureus* antigens induced up-regulation of the TNF and LTβ proteins in the spleen (Figure 6E, immunoblot; and Figure S6C, ELISA). This increased expression of LT could not, however, restore the reduced expression of the MAdCAM-1 and CXCL13 proteins in WT mice that had been pretreated for 2 wks with LTβR-Fc. Because *Igh6*$^{-/-}$ and *Rag1*$^{-/-}$ mice also manifest strongly reduced expression of CXCL13 (Ngo et al., 1999) but appear to have a normal MS (Figure S7), the reduction in CXCL13 that is observed in mice that have been treated with LTβR-Fc appears not to contribute to the changes in MS structure that are induced by treatment with this blocking reagent. We suggest, therefore, that the $CD11b^+$ cell phenotype observed following treatment with LTβR-Fc might be a result of the loss of the expression of MAdCAM-1 at the MS border leading to disrupted MS endothelial structures and consequent abnormal localization of $CD11b^+$ cells from the MZ to the WP.

Discussion

Vascular endothelial cells in different structural compartments of the mouse spleen can be distinguished based on their selective expression of specific surface antigens. Here, we found that VE-cadherin and PECAM-1 were expressed broadly on splenic endothelial cells in both the RP and the WP areas, whereas MAdCAM-1, ephrinB2, and Flk-1 were predominantly expressed by the endothelial cells of the MS. The pattern of Flk-1 expression was very similar to that reported for the molecularly undefined IBL-7/1 antigen (Balazs et al., 2001; Balogh et al., 2007), suggesting that the Flk-1^+ cells of the MS may also express the IBL-7/1 antigen. The Flk-1 antigen is particularly valuable for analysis of the development of the normal spleen MS structure because, unlike the prototypic MS marker MAdCAM-1, its expression is not dependent on the $LT\alpha_1\beta_2$ heterotrimer.

Using Flk-1, we observed that $LT\alpha_1\beta_2$ was a key signal for the establishment of normal MS structure in the postnatal period (summarized in Figure S8). The requirement for $LT\alpha_1\beta_2$ signaling was seen as early as day 3 after birth. In either *Lta*$^{-/-}$, *Ltbr*$^{-/-}$, or LTβR-Fc-treated mice, the proper organization of the endothelial cells and smooth muscle cells that form a mature MS endothelial network was disturbed. The cellular source(s) of the $LT\alpha_1\beta_2$ that drives MS development and maintenance remain undefined. We have established that the $LT\alpha_1\beta_2$ signal on cells of the lymphocyte lineage was not sufficient. Furthermore, spleens from *Rorc (γt)*$^{-/-}$ mice, which are congenitally deficient of lymphoid tissue inducer cells (LTi) (Eberl et al., 2004) and neonatal WT mice treated with anti-CD4, which depletes LTi, showed normal MS organization (data not shown). Thus, the $LT\alpha_1\beta_2$ signal is likely delivered by a non-lymphocyte bone marrow-derived cell, an immature lymphocyte or by a nearby non-hematopoietic lineage cell such as a neighboring endothelial cell. We have also demonstrated that primary mouse splenic endothelial cells and the bEnd.3 cell line expressed the LTβR and that downstream LTβR signals, such as the up-regulation of MAdCAM-1, can contribute to their reorganization. All together, our data suggest that LTβR-dependent MAdCAM-1 expression on the splenic marginal sinus endothelium may act to assist in development and maintenance of the complex MS vasculature, helping to signal its differentiation into a flattened endothelium that controls the normal distribution and trafficking of specific immune cells between the different splenic compartments.

Our ability to stain thick spleen sections (100–120 μm) has permitted us to compile three-dimensional images of the spleen vasculature, enabling us to identify unique features of the mouse MS. In particular, we showed that the MS endothelial structures did not completely surround the WP nodules, but instead they formed a complex network of vascular channels,

with flattened surfaces and multiple gaps. The structure of the MS suggests it may be adapted to reduce the rapid rate of blood flow from the central arteriole thereby allowing for enhanced interaction between resident MZ immune cells and antigen in the blood. Furthermore, the open spaces between the interconnecting MS vessels may allow for strategic positioning of macrophage and dendritic cell processes to assist in their interactions with blood borne antigens. We found that administration of LTβR-Fc to adult mice suppresses MAdCAM-1 expression, MS organization, and the normal localization of $CD11b^+$ cells that are usually exclusively in the RP following i.v. challenge with bacterial antigens. Similarly, *S1pr3*$^{-/-}$*(S1P3-deficient)* mice have disorganized MAdCAM-1 expression at the MS and showed faster migration of MZ B cells into the WP in response to LPS compared to WT (Girkontaite et al., 2004). Together these data suggest that appropriate localization of immune cells in the WP depends on the normal organization of the MS vessels.

LT and TNF family members also play key roles in maintaining the resident immune cells that are present in the MZ area. The adhesion molecules ICAM-1 and VCAM-1 play a role in the retention of MZ B cells within this compartment (Lu and Cyster, 2002), with expression of ICAM-1 and VCAM-1 on the MS endothelium controlled by signals delivered through the LTβR. Using ELISA and immunoblot, we found that expression of ICAM-1 and VCAM-1 protein, although reduced by treatment with the LTβR-Fc in adult mice, could be up-regulated in response to bacterial antigens that induce signaling via TNF and $LT\alpha_1\beta_2$. In comparison, expression of MAdCAM-1 protein was dramatically suppressed for up to 3 wks after treatment with LTβR-Fc and expression of the MAdCAM-1 protein was not up-regulated by local signals produced by the TNF or $LT\alpha_1\beta_2$ that is induced by bacterial antigens. In view of these data, it is possible that LTβR-dependent expression of MAdCAM-1 acts to maintain the integrity of the splenic endothelial structures, thereby affecting the distribution of other adhesion molecules on the MS endothelium.

We observed a correlation between the extent of disturbed MS architecture and the ability to sustain a normal distribution of macrophages in the MZ in mice that are deficient in certain of the LT and TNF family members. For example, *Lta*$^{-/-}$, *Ltb*$^{-/-}$, *Ltbr*$^{-/-}$ and *Map3k14*$^{-/-}$ mice, which have grossly disturbed MS development, all manifest a complete loss of macrophages from their normal location in the MZ. *Tnf*$^{-/-}$ and *Tnfrs1a*$^{-/-}$ mice, on the other hand, which retain substantial MS structure, show instead reduced numbers of macrophages that maintain an apparently normal distribution in the MZ (Banks et al., 1995; De Togni et al., 1994; Futterer et al., 1998; Pasparakis et al., 2000). As demonstrated in this paper, the failure of MAdCAM-1 up-regulation and of reorganization of $Flk\text{-}1^+$ vessels during postnatal development in the spleens of *Lta*$^{-/-}$ and *Ltbr*$^{-/-}$ mice leads to a profound loss of a normal complex MS endothelial cell network in adult animals. In contrast, MAdCAM-1 expression, although reduced in intensity, was present in the developing spleens of *Tnf*$^{-/-}$ and *Tnfrsf1a*$^{-/-}$ mice. As postnatal spleen development progressed in these TNF- and TNFRI-targeted mice, expression of MAdCAM-1 on the MS remained reduced. In adult mice of these strains, however, MAdCAM-1 was dramatically suppressed with few $MAdCAM\text{-}1^+$ cells (which may represent residual FDCs; data not shown) found in the marginal zone. Therefore, the substantial reduction of MAdCAM-1 expression in adult spleens of *Tnf*$^{-/-}$ and *Tnfrsf1a*$^{-/-}$ mice may contribute to their irregular MS phenotype. The association between the failure of macrophage localization to the MS in *Lta*$^{-/-}$ and *Ltbr*$^{-/-}$ mice and the profound loss of MS structural complexity in these strains, together with the less severe reduction in MS macrophages and only a partial MS structural defect in *Tnf*$^{-/-}$ and *Tnfrsf1a*$^{-/-}$ mice supports our hypothesis that the proper organization of this unique vascular structure directly affects the positioning and/or numbers of resident immune cells in the MZ area.

Our studies demonstrate that interactions between $LT\alpha_1\beta_2$ and the LTβR, both during the neonatal period and in adult mice, regulate MAdCAM-1 expression and normal MS

organization. *In vitro*, endothelial cells utilize LTβR signals and MAdCAM-1 expression to reorganize and form flattened structures implicating MAdCAM-1 as a mediator of the development and maintenance of a normal MS network. Experiments using *in vivo* treatment with an MAdCAM-1 mAb (MECA-367) that blocks adhesive interactions with β7 integrins either alone or in combination with a blocking VCAM-1 mAb (data not shown) did not alter the normal pattern of MS vascular development. Furthermore, *Itgb7*$^{-/-}$ (integrin β7-deficient) mice appear to have a normal MZ structure (Lu and Cyster, 2002). Together these studies suggest that the N-terminal Ig domain of MAdCAM-1 (the molecular target of the MECA-367 mAb) which typically interacts with the integrin α4β7 does not contribute to MS organization. Our *in vitro* data show that MAdCAM-1 localizes to the plasma membrane at the apical and basal surfaces of the cell and thus may be in tight association with the extracellular matrix *in vivo*. Therefore, MAdCAM-1 may play a central role in the establishment of the normal MS network by using either another N-terminal Ig domain or its mucin domain, which is physically distinct from the MECA-367 epitope. Future studies using transgenic and gene targeted mice affecting selective domains of MAdCAM-1 will be required to determine the molecular details of how this adhesion molecule contributes to the establishment and maintenance of mature MS organization.

Experimental Procedures

Mice

C57BL/6J, *Igh6*$^{-/-}$, *Rag1*$^{-/-}$, *Tcrb*$^{-/-}$*Tcrd*$^{-/-}$ mice (Jackson Labs), *Il15*$^{-/-}$ mice (Taconic), Efnb2$^{+/-}$ (Wang et al., 1998), *Efnb2*$^{+/-}$ × *Lta*$^{-/-}$ (129/C57BL/6), *Lta*$^{-/-}$ (C57BL/6) (De Togni et al., 1994), *Tnfrsf1a*$^{-/-}$ (Pasparakis et al., 1997), *Ltbr*$^{-/-}$ (Futterer et al., 1998), *Map3k14*$^{-/-}$ (129/SvEv) (Yin et al., 2001), and *Icam1*^{null} mice (Bullard et al., 2007) were housed in specific pathogen free facilities at Washington University and at the University of Alabama at Birmingham. Adult mice were used at 6–10 wks of age. Frozen spleen from an *Rorc(γt)* mouse was provided courtesy of Dr. Daniel Littman (Eberl et al., 2004). Animal use was approved by the Institutional Animal Care and Use Committees of Washington University and the University of Alabama at Birmingham.

Tissue Preparation

Spleens processed for conventional two-dimensional imaging were embedded in O.C.T. Compound (Tissue-Tek) and frozen with 2-methyl butane chilled with liquid nitrogen. Tissue sections (10μm or 20 μm thick) were melted onto glass slides, dried, and fixed in cold acetone for 10 mins prior to storage at −20°C. Sections used for staining with an anti-β-gal antibody were fixed in 4% paraformaldehyde (PFA) for 5 minutes at room temperature and then in cold acetone for 5 mins. Sections requiring quenching were incubated with 0.3% H_2O_2 in PBS for 3–5 mins. All immunostaining steps were performed at room temperature.

Spleens processed for thick section and three-dimensional imaging were fixed in 2% PFA, washed in PBS, and then cushioned in 30% sucrose. Whole tissue was then frozen in M1 matrix medium (ThermoShandon) on the chilled stage of a sliding microtome (American Optical Corp., model 860). Tissue sections were cut at 120 μm, placed in cold PBS, and permeabilized with cold acetone (−20°C) prior to antibody staining at 4°C.

Reagents for Immunostaining and Immunoblotting

The following reagents were used for immunostaining: anti-Flk1 (VEGF-R2), anti-MAdCAM-1 (MECA-367), anti-PECAM-1 (CD31), anti-VE-Cadherin (CD144), anti-B220, anti-IgM, anti-CD3ε, anti-Thy1.2, anti-CD11b, anti-rat Ig biotin, and anti-rat IgM PE (BD Biosciences); anti-smooth muscle actin (SMA), Streptavidin (SA)-Quantum Red, anti-FLAG (M2) and the Fast 3,3-DAB reagent (Sigma-Aldrich); MOMA-1 antibody (Serotec); SA-Alexa

350, SA-Alexa 488, anti-rabbit Ig-Alexa 488, anti-fluorescein Alexa 488, Hoechst dye and the Prolong Antifade kit (Invitrogen); SA-alkaline phosphatase (AP) (Southern Biotech); anti-FITC-horse radish peroxidase (HRP) (Dako); anti-β-galactosidase (Cortex Biochem); anti-LTβR (Santa Cruz) and Vector blue substrate (Vector Labs). The anti-Flk-1, anti-CD31, anti-β-galactosidase and anti-MAdCAM-1 (MECA-367) were conjugated with HRP using the Roche Peroxidase Labeling kit. The HRP-labeled antibodies were visualized with the Tyramide Amplification System (NEN).

The following reagents were used for immunoblotting: anti-TNF, anti-ICAM-1, anti-VCAM-1, anti-CXCL13-biotin, and anti-CCL21-biotin (R&D Systems); anti-MAdCAM-1 (MECA-367, BD Biosciences); anti-β-actin and anti-FLAG (M2) (Sigma); anti-LTβR (Santa Cruz); peroxidase-conjugated (POD) anti-goat Ig, POD anti-mouse Ig, POD anti-rat Ig, POD anti-biotin and POD SA (Roche or Zymed); biotinylated anti-hamster-Ig (Jackson ImmunoResearch); and the hamster anti-mouse LTβ BBF6 (generously provided by Jeff Browning and Biogen Idec) (Browning et al., 1997).

Microscopes and Imaging Systems

Images from conventional 10–20 μm thick sections were captured with an Olympus BX60 microscope using an Optronics cooled CCD digital camera. The individual fluorescent images were compiled using Adobe Photoshop. Images of cultured cells were captured with a Zeiss Axiovert 25 microscope and AxioCam HRc camera. Quantitative analysis of fluorescent images was performed with the NIH Image J software. Data were expressed as means +/− SE and statistical analyses were performed using the two-tailed Student's t-test with two-sample unequal variance.

Images for the co-localization studies were captured with a Zeiss LSM 510 inverted microscope and the Zeiss LSM 5 software. The thick sections and three-dimensional images were captured at the High Resolution Imaging Facility at the University of Alabama at Birmingham (UAB) with a Leica DMIRBE inverted epifluorescence microscope outfitted with Leica TCS NT Laser Confocal optics (Leica, Inc.; Exton, PA). Optical sections through the Z axis was generated using a stage galvanometer or step motor. Flattened maximum projections of image stacks were prepared using Leica's proprietary confocal imaging software.

In Vivo Administration of Proteins

Adult mice were administered 100 μg of either human IgG1 or LTβR-Fc via i.p. injection and sacrificed 2 wks later. The murine LTβR-Fc (constructed using a human IgG1 Fc fragment) was generously provided by Jeff Browning and Biogen Idec (Browning et al., 1995) and the control human IgG was purchased from Sigma. *S. aureus* bioparticles from Invitrogen (either unlabeled or TMR-labeled) were administered by i.v. injection at 3, 12 and 24 hours before sacrifice.

Immunoblotting

Spleen tissue was disrupted with a Dounce homogenizer (Sigma) in 50:50 T-Per lysis solution (Pierce): RIPA lysis buffer (1% NP40, 50 mM Tris-HCl pH 8, 150 mM NaCl, 0.5% deoxycholate, 0.1% SDS) plus 0.1% Protease Inhibitor Cocktail (Sigma). Cells in suspension or grown on plastic were lysed with RIPA buffer containing protease inhibitors. Cells were lysed for subcellular protein fractionation using the S-PEK kit (Calbiochem). The lysates were clarified by centrifugation for 10 mins at 4°C in a microfuge. Protein content of the lysates was determined using the BioRad DC protein assay kit and then samples were boiled for 5 mins in 2× sample buffer (0.5M Tris-HCl pH 6.8, 0.4% SDS, 20% glycerol, 0.3% Bromophenol blue) prior to SDS polyacrylamide gel electrophoresis. Proteins were transferred to nitrocellulose (BioRad), membranes were blocked with 5% non-fat milk in Tris-buffered saline (TBS), and

the blots were probed with the primary antibody in blocking buffer for 1–2 hours at room temperature or overnight at 4°C prior to washing 4 times for 10 mins each with TBS + 1% Tween-20 (TBST). Filters were incubated for 45–60 mins with the secondary antibody in blocking buffer followed by washing with TBST 4 times for 15 mins each and then developed using a chemiluminescence detection kit (Roche).

ELISA

Quantikine colorimetric sandwich ELISA and DuoSet kits were from R&D Systems. For the MAdCAM-1 DuoSet, we used 1 μg/ml of the MAdCAM-1 (MECA367) antibody from BD biosciences for coating Immunlon 4HBX plates (Thermo Scientific) and if needed, diluted the protein samples in Reagent Diluent 1 (R&D Systems DY997). Data were expressed as means +/− SE and statistical analyses were performed using the two-tailed Student's t-test with two-sample unequal variance.

RT-PCR

RNA was isolated with the RNeasy kit (Qiagen) and RT-PCR was performed using the Titan one-step RT-PCR kit (Roche). The primers for LTβR were GTATGCAGCCGCAGCCAAG (forward) and AGTAGGAGGTACCTGGAGCTGCC (reverse). The primers for β-actin were TCGTGCGTGACATCAAAGAG (forward) and TGGACAGTGAGGCCAGGATG (reverse).

Cell culture

The bEnd.3 mouse brain endothelial cell line, mouse TIMI.4 thymoma line, and L929 mouse fibroblast cell line (ATCC) were grown in DMEM containing 10% FBS (Hyclone) and 1% penicillin/streptomycin (Invitrogen). Isolated spleen endothelial cells were cultured in EGM-2 MV media with growth factor additives (Lonza) and supplemented with 1 μmol/L of a smooth muscle cell inhibitor (Calbiochem). Cells were cultured either on collagen-coated glass 4-well chamber slides (BD Biosciences) for AcLDL-Alexa488 (Invitrogen) uptake or plated on 200 μl of Matrigel (BD Biosciences) in a 24-well plate at 2×10^5 cells per well. Cells were also grown on Matrigel-coated Anapore filters (Fisher), fixed in 2% PFA, washed in PBS, cushioned in 30% sucrose, and then frozen in O.C.T. Cells treated with antibodies were given either 0.5 μg/ml of a control hamster Ig (PIP-1D1; anti-glutathione S transferase (Mandik-Nayak et al., 2001) or agonist hamster anti-mouse LTβR (AF.H6) kindly provided by Jeff Browning and Biogen Idec (Rennert et al., 1998).

Splenic endothelial cell isolation

Cells from 10 spleens were pooled for each endothelial cell preparation to seed 1 well of a 24-well plate or 1 well of a 4-well chamber slide. The spleens were first gently broken up between the frosted ends of 2 sterile glass slides to release the majority of the red and white blood cells which were then discarded. The remaining mass of tissue was digested with 5 mg/ml Collagenase D (Roche) and 2 mg/ml DNase I (Sigma) in a 37°C water bath for 45 mins. The tissue was gently vortexed for 20 secs every 15 mins. The digested material was then passed through a 40 μm filter and the resulting single cell suspension was washed in MACS buffer (PBS/2%FBS/2mM EDTA). The cells were incubated with anti-Flk-1 or anti-CD144 (BD Biosciences), followed by incubation with anti-rat Ig-MACS beads (Miltenyi Biotec) and positively selected on a magnetic MACS column.

Expression vectors and transient transfections

Murine MAdCAM-1 cDNA corresponding to nt 21 to 1243 (NM_013591) was amplified from bEND.3 mRNA with the Expand High Fidelity Plus PCR system (Roche). Purified PCR fragments were then subcloned into the p3xFLAG-CMV-14 vector (Sigma). bEnd.3 cells were

transfected with AMAXA Basic Nucleofector Kit Primary Endothelial Cells using program T-020 according to the manufacturer's protocol. bEnd.3 cells were then rested overnight in 60 mm dishes prior to analysis or plating on Matrigel.

Supplementary Material

Refer to Web version on PubMed Central for supplementary material.

Acknowledgments

We thank Dr. J. Browning and Biogen Idec for providing the LTβR-Fc, the agonist anti-LTβR and the BBF6 monoclonal Ab, Dr. J. Anderson for the *Efnb2*$^{+/-}$ mice, Dr. K. Pfeffer for the *Ltbr*$^{-/-}$ mice, Dr. D. Bullard for the *Icam1*^{null} mice, and Dr. D. Littman for spleen from the *Rorc(γt)* mice. We also thank Drs. D. Randolph and J. Deshane for valuable comments on the manuscript. Finally, we are grateful to Dr. K. Keyser and the staff of the High Resolution Imaging Facility at the University of Alabama at Birmingham. In particular, Albert Tousson provided invaluable assistance on confocal imaging and many helpful discussions, and Tammy Bailey assisted with the sliding microtome. During the initial phases of this work, Dr. Chaplin was an investigator of the Howard Hughes Medical Institute.

References

Balazs M, Horvath G, Grama L, Balogh P. Phenotypic identification and development of distinct microvascular compartments in the postnatal mouse spleen. Cell Immunol 2001;212:126–137. [PubMed: 11748929]

Balazs M, Martin F, Zhou T, Kearney J. Blood dendritic cells interact with splenic marginal zone B cells to initiate T-independent immune responses. Immunity 2002;17:341–352. [PubMed: 12354386]

Balogh P, Balazs M, Czompoly T, Weih DS, Arnold HH, Weih F. Distinct roles of lymphotoxin-beta signaling and the homeodomain transcription factor Nkx2.3 in the ontogeny of endothelial compartments in spleen. Cell Tissue Res 2007;328:473–486. [PubMed: 17318587]

Banks TA, Rouse BT, Kerley MK, Blair PJ, Godfrey VL, Kuklin NA, Bouley DM, Thomas J, Kanangat S, Mucenski ML. Lymphotoxin-alpha-deficient mice. Effects on secondary lymphoid organ development and humoral immune responsiveness. J Immunol 1995;155:1685–1693. [PubMed: 7636227]

Bohnsack JF, Brown EJ. The role of the spleen in resistance to infection. Annu Rev Med 1986;37:49–59. [PubMed: 3518612]

Browning JL, Dougas I, Ngam-ek A, Bourdon PR, Ehrenfels BN, Miatkowski K, Zafari M, Yampaglia AM, Lawton P, Meier W, et al. Characterization of surface lymphotoxin forms. Use of specific monoclonal antibodies and soluble receptors. J Immunol 1995;154:33–46. [PubMed: 7995952]

Browning JL, Sizing ID, Lawton P, Bourdon PR, Rennert PD, Majeau GR, Ambrose CM, Hession C, Miatkowski K, Griffiths DA, et al. Characterization of lymphotoxin-alpha beta complexes on the surface of mouse lymphocytes. J Immunol 1997;159:3288–3298. [PubMed: 9317127]

Bullard DC, Hu X, Schoeb TR, Collins RG, Beaudet AL, Barnum SR. Intercellular adhesion molecule-1 expression is required on multiple cell types for the development of experimental autoimmune encephalomyelitis. J Immunol 2007;178:851–857. [PubMed: 17202346]

De Togni P, Goellner J, Ruddle NH, Streeter PR, Fick A, Mariathasan S, Smith SC, Carlson R, Shornick LP, Strauss-Schoenberger J, et al. Abnormal development of peripheral lymphoid organs in mice deficient in lymphotoxin. Science 1994;264:703–707. [PubMed: 8171322]

Dejardin E, Droin NM, Delhase M, Haas E, Cao Y, Makris C, Li ZW, Karin M, Ware CF, Green DR. The lymphotoxin-beta receptor induces different patterns of gene expression via two NF-kappaB pathways. Immunity 2002;17:525–535. [PubMed: 12387745]

Eberl G, Marmon S, Sunshine MJ, Rennert PD, Choi Y, Littman DR. An essential function for the nuclear receptor RORgamma(t) in the generation of fetal lymphoid tissue inducer cells. Nat Immunol 2004;5:64–73. [PubMed: 14691482]

Ejstrud P, Kristensen B, Hansen JB, Madsen KM, Schonheyder HC, Sorensen HT. Risk and patterns of bacteraemia after splenectomy: a population-based study. Scand J Infect Dis 2000;32:521–525. [PubMed: 11055658]

Ettinger R, Browning JL, Michie SA, van Ewijk W, McDevitt HO. Disrupted splenic architecture, but normal lymph node development in mice expressing a soluble lymphotoxin-beta receptor-IgG1 fusion protein. Proc Natl Acad Sci U S A 1996;93:13102–13107. [PubMed: 8917551]

Fu YX, Chaplin DD. Development and maturation of secondary lymphoid tissues. Annu Rev Immunol 1999;17:399–433. [PubMed: 10358764]

Futterer A, Mink K, Luz A, Kosco-Vilbois MH, Pfeffer K. The lymphotoxin beta receptor controls organogenesis and affinity maturation in peripheral lymphoid tissues. Immunity 1998;9:59–70. [PubMed: 9697836]

Gale NW, Baluk P, Pan L, Kwan M, Holash J, DeChiara TM, McDonald DM, Yancopoulos GD. Ephrin-B2 selectively marks arterial vessels and neovascularization sites in the adult, with expression in both endothelial and smooth-muscle cells. Dev Biol 2001;230:151–160. [PubMed: 11161569]

Girkontaite I, Sakk V, Wagner M, Borggrefe T, Tedford K, Chun J, Fischer KD. The sphingosine-1-phosphate (S1P) lysophospholipid receptor S1P3 regulates MAdCAM-1+ endothelial cells in splenic marginal sinus organization. J Exp Med 2004;200:1491–1501. [PubMed: 15583019]

Grayson MH, Chaplin DD, Karl IE, Hotchkiss RS. Confocal fluorescent intravital microscopy of the murine spleen. J Immunol Methods 2001;256:55–63. [PubMed: 11516755]

Karlsson MC, Guinamard R, Bolland S, Sankala M, Steinman RM, Ravetch JV. Macrophages control the retention and trafficking of B lymphocytes in the splenic marginal zone. J Exp Med 2003;198:333–340. [PubMed: 12874264]

Koike R, Nishimura T, Yasumizu R, Tanaka H, Hataba Y, Hataba Y, Watanabe T, Miyawaki S, Miyasaka M. The splenic marginal zone is absent in alymphoplastic aly mutant mice. Eur J Immunol 1996;26:669–675. [PubMed: 8605936]

Koni PA, Sacca R, Lawton P, Browning JL, Ruddle NH, Flavell RA. Distinct roles in lymphoid organogenesis for lymphotoxins alpha and beta revealed in lymphotoxin beta-deficient mice. Immunity 1997;6:491–500. [PubMed: 9133428]

Kraal G. Cells in the marginal zone of the spleen. Int Rev Cytol 1992;132:31–74. [PubMed: 1555921]

Kraal G, Janse M. Marginal metallophilic cells of the mouse spleen identified by a monoclonal antibody. Immunology 1986;58:665–669. [PubMed: 3733156]

Kraal G, Mebius R. New insights into the cell biology of the marginal zone of the spleen. Int Rev Cytol 2006;250:175–215. [PubMed: 16861066]

Kraal G, Schornagel K, Streeter PR, Holzmann B, Butcher EC. Expression of the mucosal vascular addressin, MAdCAM-1, on sinus-lining cells in the spleen. Am J Pathol 1995;147:763–771. [PubMed: 7677187]

Lo JC, Basak S, James ES, Quiambo RS, Kinsella MC, Alegre ML, Weih F, Franzoso G, Hoffmann A, Fu YX. Coordination between NF-kappaB family members p50 and p52 is essential for mediating LTbetaR signals in the development and organization of secondary lymphoid tissues. Blood 2006;107:1048–1055. [PubMed: 16195333]

Lu TT, Cyster JG. Integrin-mediated long-term B cell retention in the splenic marginal zone. Science 2002;297:409–412. [PubMed: 12130787]

Mackay F, Majeau GR, Lawton P, Hochman PS, Browning JL. Lymphotoxin but not tumor necrosis factor functions to maintain splenic architecture and humoral responsiveness in adult mice. Eur J Immunol 1997;27:2033–2042. [PubMed: 9295042]

Mandik-Nayak L, Huang G, Sheehan KC, Erikson J, Chaplin DD. Signaling through TNF receptor p55 in TNF-alpha-deficient mice alters the CXCL13/CCL19/CCL21 ratio in the spleen and induces maturation and migration of anergic B cells into the B cell follicle. J Immunol 2001;167:1920–1928. [PubMed: 11489971]

Matsushima A, Kaisho T, Rennert PD, Nakano H, Kurosawa K, Uchida D, Takeda K, Akira S, Matsumoto M. Essential role of nuclear factor (NF)-kappaB-inducing kinase and inhibitor of kappaB (IkappaB) kinase alpha in NF-kappaB activation through lymphotoxin beta receptor, but not through tumor necrosis factor receptor I. J Exp Med 2001;193:631–636. [PubMed: 11238593]

Mebius RE, Kraal G. Structure and function of the spleen. Nat Rev Immunol 2005;5:606–616. [PubMed: 16056254]

Mebius RE, Nolte MA, Kraal G. Development and function of the splenic marginal zone. Crit Rev Immunol 2004;24:449–464. [PubMed: 15777163]

Mebius RE, Streeter PR, Michie S, Butcher EC, Weissman IL. A developmental switch in lymphocyte homing receptor and endothelial vascular addressin expression regulates lymphocyte homing and permits CD4+ CD3− cells to colonize lymph nodes. Proc Natl Acad Sci U S A 1996;93:11019–11024. [PubMed: 8855301]

Neumann B, Luz A, Pfeffer K, Holzmann B. Defective Peyer's patch organogenesis in mice lacking the 55-kD receptor for tumor necrosis factor. J Exp Med 1996;184:259–264. [PubMed: 8691140]

Ngo VN, Korner H, Gunn MD, Schmidt KN, Riminton DS, Cooper MD, Browning JL, Sedgwick JD, Cyster JG. Lymphotoxin alpha/beta and tumor necrosis factor are required for stromal cell expression of homing chemokines in B and T cell areas of the spleen. J Exp Med 1999;189:403–412. [PubMed: 9892622]

Pasparakis M, Alexopoulou L, Episkopou V, Kollias G. Immune and inflammatory responses in TNF alpha-deficient mice: a critical requirement for TNF alpha in the formation of primary B cell follicles, follicular dendritic cell networks and germinal centers, and in the maturation of the humoral immune response. J Exp Med 1996;184:1397–1411. [PubMed: 8879212]

Pasparakis M, Alexopoulou L, Grell M, Pfizenmaier K, Bluethmann H, Kollias G. Peyer's patch organogenesis is intact yet formation of B lymphocyte follicles is defective in peripheral lymphoid organs of mice deficient for tumor necrosis factor and its 55-kDa receptor. Proc Natl Acad Sci U S A 1997;94:6319–6323. [PubMed: 9177215]

Pasparakis M, Kousteni S, Peschon J, Kollias G. Tumor necrosis factor and the p55TNF receptor are required for optimal development of the marginal sinus and for migration of follicular dendritic cell precursors into splenic follicles. Cell Immunol 2000;201:33–41. [PubMed: 10805971]

Rennert PD, Browning JL, Mebius R, Mackay F, Hochman PS. Surface lymphotoxin alpha/beta complex is required for the development of peripheral lymphoid organs. J Exp Med 1996;184:1999–2006. [PubMed: 8920886]

Rennert PD, James D, Mackay F, Browning JL, Hochman PS. Lymph node genesis is induced by signaling through the lymphotoxin beta receptor. Immunity 1998;9:71–79. [PubMed: 9697837]

Schmidt EE, MacDonald IC, Groom AC. Microcirculation in mouse spleen (nonsinusal) studied by means of corrosion casts. Journal of Morphology 1985;186:17–29.

Shin D, Garcia-Cardena G, Hayashi S, Gerety S, Asahara T, Stavrakis G, Isner J, Folkman J, Gimbrone MA Jr, Anderson DJ. Expression of ephrinB2 identifies a stable genetic difference between arterial and venous vascular smooth muscle as well as endothelial cells, and marks subsets of microvessels at sites of adult neovascularization. Dev Biol 2001;230:139–150. [PubMed: 11161568]

Smith C, Andreakos E, Crawley JB, Brennan FM, Feldmann M, Foxwell BM. NF-kappaB-inducing kinase is dispensable for activation of NF-kappaB in inflammatory settings but essential for lymphotoxin beta receptor activation of NF-kappaB in primary human fibroblasts. J Immunol 2001;167:5895–5903. [PubMed: 11698466]

Steiniger B, Barth P. Microanatomy and function of the spleen. Adv Anat Embryol Cell Biol 2000;151:III–IX. 1–101. [PubMed: 10592524]

Waghorn DJ. Overwhelming infection in asplenic patients: current best practice preventive measures are not being followed. J Clin Pathol 2001;54:214–218. [PubMed: 11253134]

Wang HU, Chen ZF, Anderson DJ. Molecular distinction and angiogenic interaction between embryonic arteries and veins revealed by ephrin-B2 and its receptor Eph-B4. Cell 1998;93:741–753. [PubMed: 9630219]

Weih DS, Yilmaz ZB, Weih F. Essential role of RelB in germinal center and marginal zone formation and proper expression of homing chemokines. J Immunol 2001;167:1909–1919. [PubMed: 11489970]

Yin L, Wu L, Wesche H, Arthur CD, White JM, Goeddel DV, Schreiber RD. Defective lymphotoxin-beta receptor-induced NF-kappaB transcriptional activity in NIK-deficient mice. Science 2001;291:2162–2165. [PubMed: 11251123]

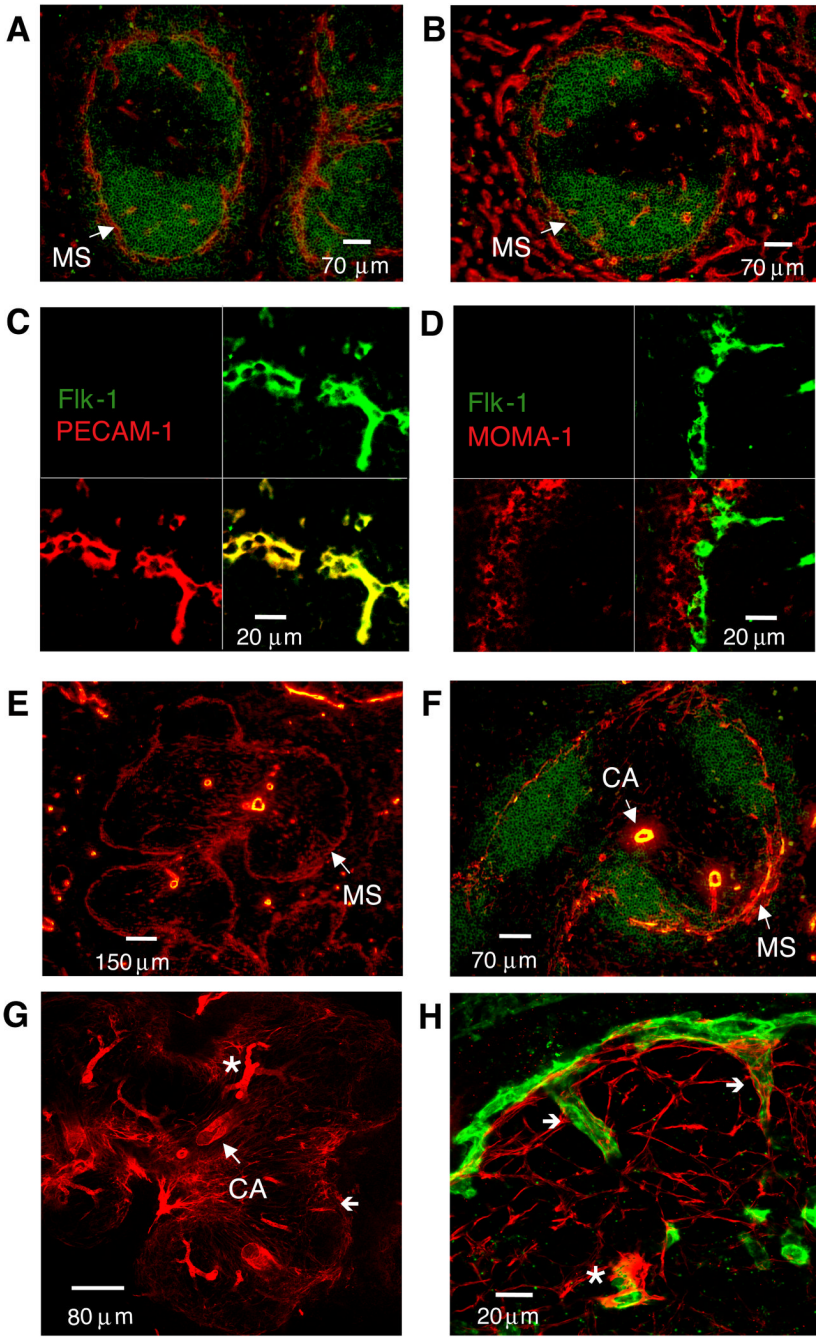

Figure 1. Flk-1 marks marginal sinus smooth muscle-associated endothelial cells in the mouse spleen

Ten μm thick frozen sections from C57BL/6 spleens (n>10) were stained with anti-B220 (green) and either (A) anti-Flk-1 (red) or (B) anti-CD144 (VE-cadherin) (red) (magnification 200×). In panels C and D, staining was with anti-Flk-1 (green) and either (C) anti-PECAM-1 (red) or (D) anti-MOMA-1 (red). For panels E and F, spleen sections were cut at 20μm and stained with (E) anti-SMA alone (red) (magnification 100×) or together with (F) anti-B220 (green) (magnification 200×). For panels G and H, staining was with (G) anti-SMA alone (red) (magnification 100×) or together with (H) anti-Flk-1 (green) (magnification 630×). For panels C, D, G, and H, confocal microscopy was used to compile a series of Z-stack images to

reconstruct a 6 μm thick section. CA, central arteriole; *, central arteriole branching vessel; (←), MS connecting vessels. Similar data were obtained in two additional experiments.

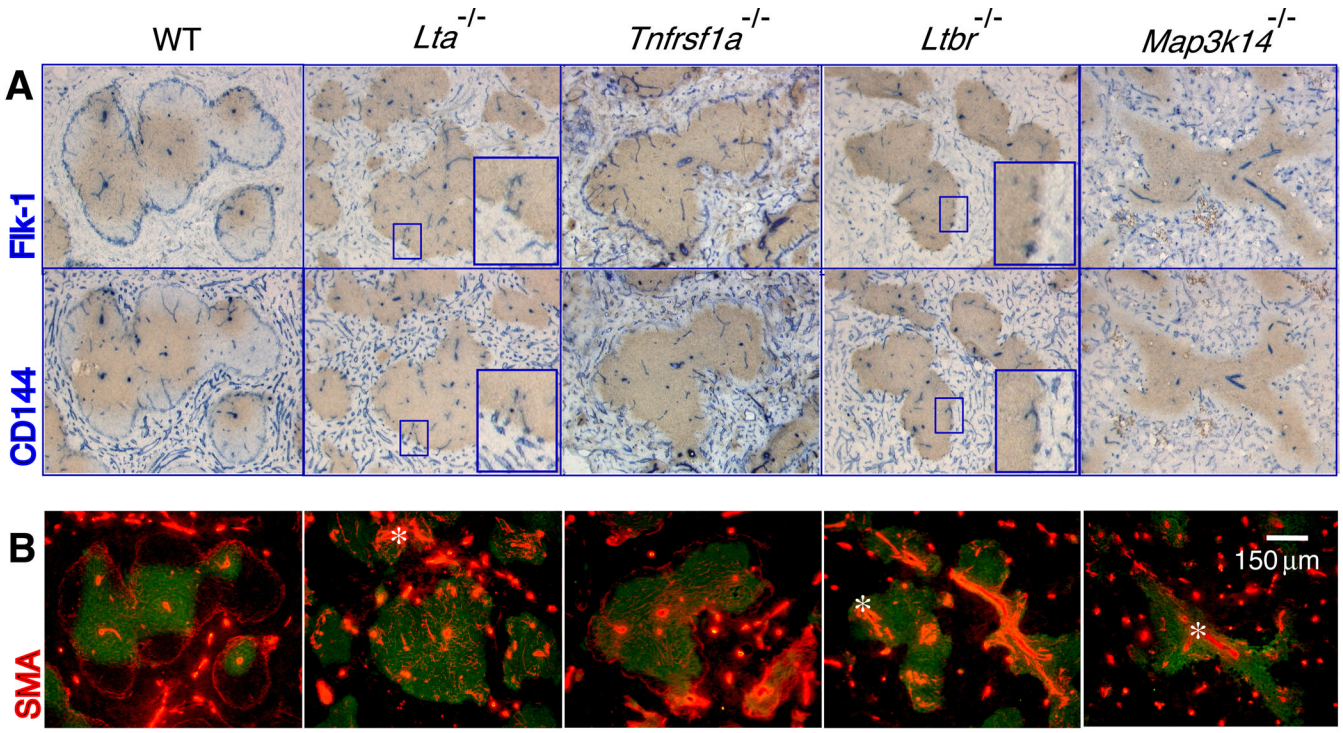

Figure 2. LTβR signaling supports the organization of endothelial and smooth muscle cells in the marginal sinus

Twenty µm thick frozen sections from spleens (n≥5) of the indicated mouse strains were stained with (A) anti-Thy1.2 (brown) and either anti-Flk-1 (blue, top panels) or anti-CD144 (VE-cadherin) (blue, bottom panels), and (B) anti-Thy1.2 (green) and anti-SMA (red) (magnification 200×). Inset images show magnified areas highlighting the Flk-1^{+} and CD144^{+} structures at the periphery of white pulp areas in the gene targeted mice.

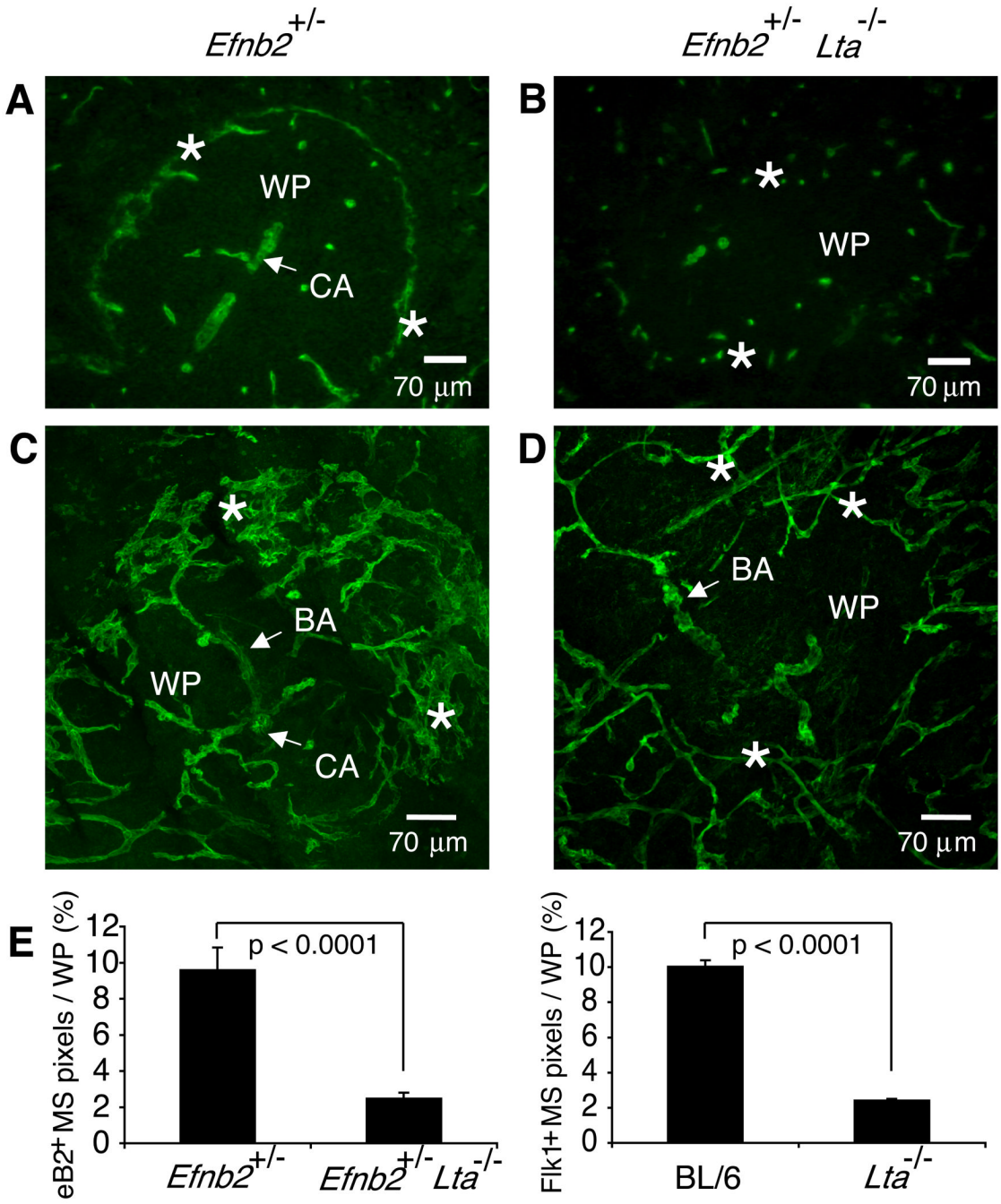

Figure 3. Disturbed MS endothelial cell network in *Lta*$^{-/-}$ mice

Spleens of *Efnb2*$^{+/-}$ (A, B) and *Efnb2*$^{+/-}$ *Lta*$^{-/-}$ (C, D) mice were cut to yield (A, C) 10 µm or (B, D) 120 µm sections and stained with anti-β-galactosidase (green) to visualize ephrinB2 expression via the expression of the in frame knock in of the LacZ gene. Confocal images were compiled to yield a 50–60 µm section of spleen, permitting analysis of the 3-D structure of a region of a single white pulp nodule (magnification 200×). Similar data were obtained by analyzing spleens from 5 additional pairs of mice. (E) The percentage of ephrinB2^{+} and Flk-1^{+} MS structures per WP area was quantified from 10 µm sections using a 20× objective. Graphs show mean + SD (n≥40 WP nodules using ≥5 spleens per strain). Data were compiled from 5 independent experiments.

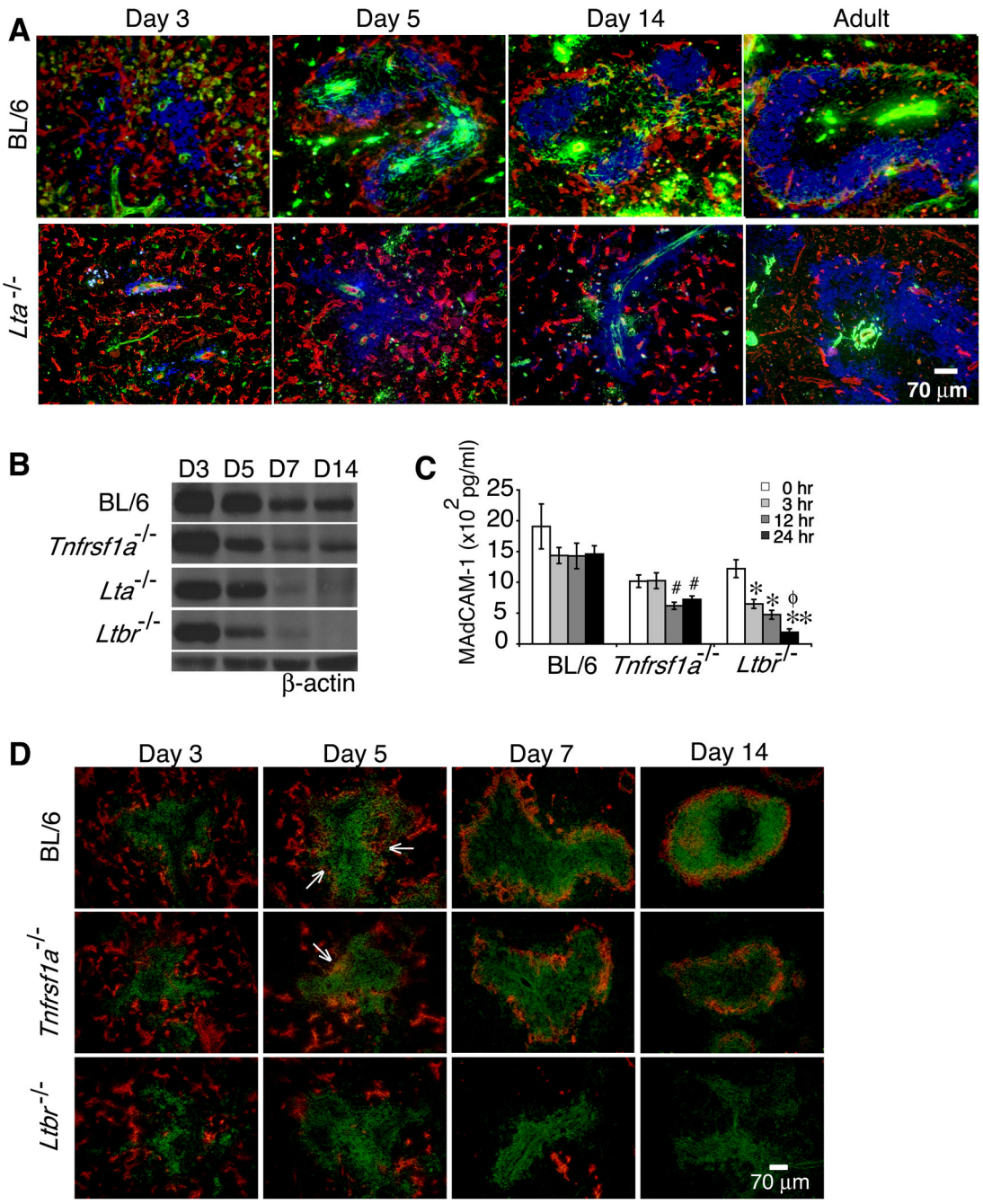

Figure 4. Lymphotoxin controls organization of Flk-1$^+$ vessels and expression of MAdCAM-1 during neonatal development

(A) Frozen sections of spleens from C57BL/6 and *Lta*$^{-/-}$ mice harvested at the indicated ages (n≥5 per strain per time point) were stained with anti-Flk-1 (red), anti-SMA (green), and anti-B220 (blue) (magnification 200×). Expression of MAdCAM-1 protein was analyzed by (B) immunoblotting and (C) ELISA from extracts of whole spleens (n=10 spleens per strain per time point) of C57BL/6, *Lta*$^{-/-}$, *Ltbr*$^{-/-}$ and *Tnfrsf1a*$^{-/-}$ mice. (D) Spleen sections from the indicated mouse strains (n=10 spleens per strain per time point) harvested on the indicated postnatal days were stained with anti-MAdCAM-1 (red) and anti-B220 (green). $^{\#}p < 0.01$ comparing C57BL/6 and *Tnfrsf1a*$^{-/-}$ mice, $^{*}p < 0.005$ and $^{**}p < 0.001$ for comparisons between

C57BL/6 and *Ltbr*$^{-/-}$ mice, and $^{\phi}$p <0.001 for comparison between *Tnfrsf1a*$^{-/-}$ and *Ltbr*$^{-/-}$ mice.

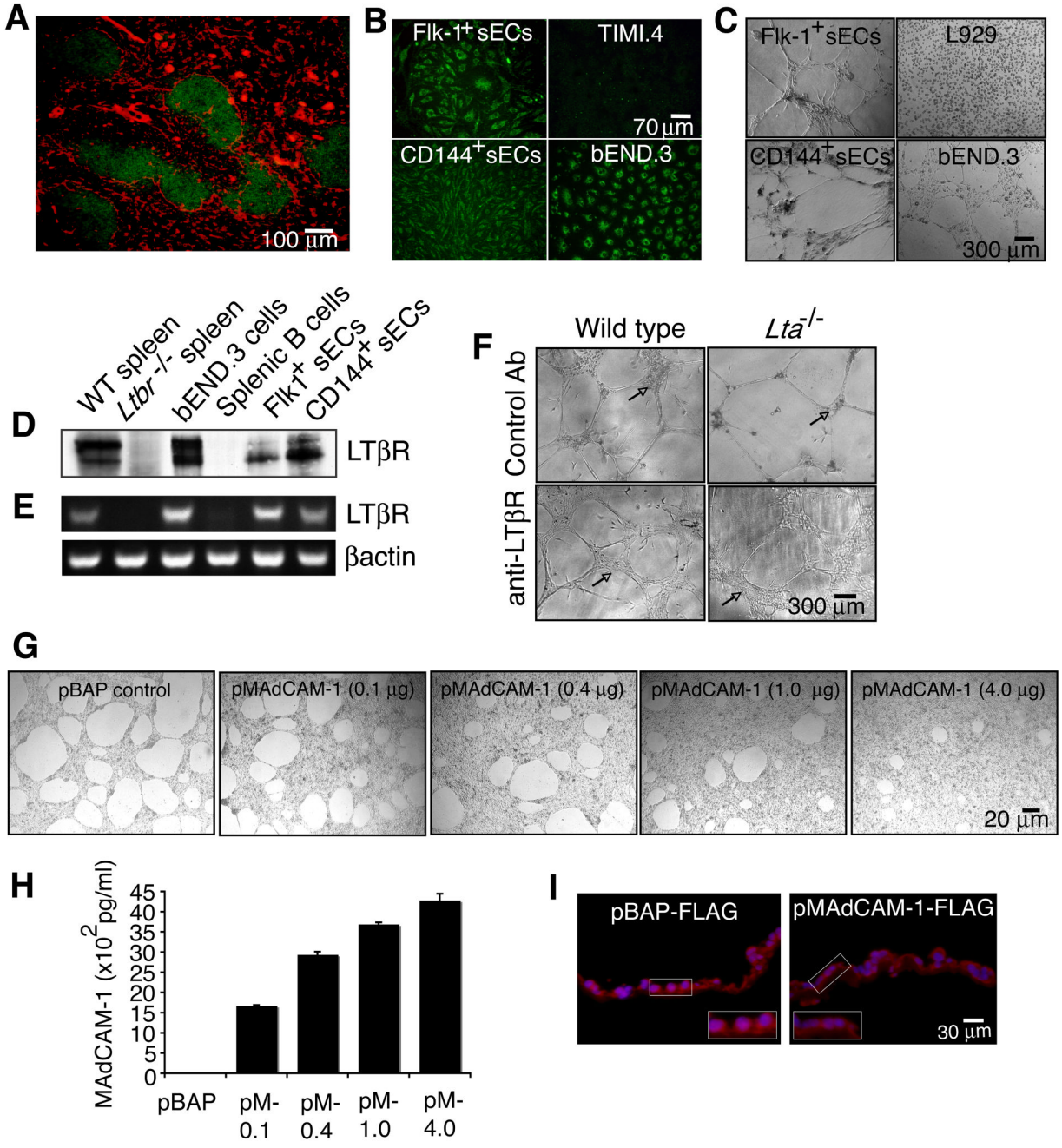

Figure 5. Endothelial cells express the LTβR and utilize MAdCAM-1 to form specialized structures on Matrigel

(A) Ten µm spleen sections from WT mice were stained with anti-LTβR (red) and anti-B220 (green) (n=3). Endothelial cells isolated from WT spleen (sECs) using either anti-Flk-1 or anti-CD144 were measured for (B) uptake of AcLDL (green) and (C) observed for formation of tube-like structures on Matrigel (n=3). sECs and the bEND.3 cell line were analyzed for expression of (D) LTβR protein and (E) RNA by immunoblotting and RT-PCR. (F) sECs isolated from WT and *Lta*$^{-/-}$ mice were plated on Matrigel containing a control GST antibody or an agonist anti-LTβR and cultured for 10 days. (G) bEND.3 cells were transfected with a control pBAP-FLAG vector (expressing bacterial alkaline phosphatase) or 0.1, 0.4, 1, and 4

μg of a pMAdCAM-1-FLAG vector. The cells were then plated on Matrigel and cultured for 24 hrs. (H) Protein extracts from transfected bEND.3 cells were prepared and an ELISA was performed to assess MAdCAM-1 protein expression. (I) Transfected bEND.3 cells grown on Anapore filters coated with Matrigel were fixed and frozen in O.C.T. and 8 μm cross-section slices were stained with anti-FLAG (red) and Hoechst (blue). Inset images show magnified areas highlighting the EC phenotype and amount of MAdCAM-1 associated with the Matrigel. Data shown are representative of 3 independent experiments.

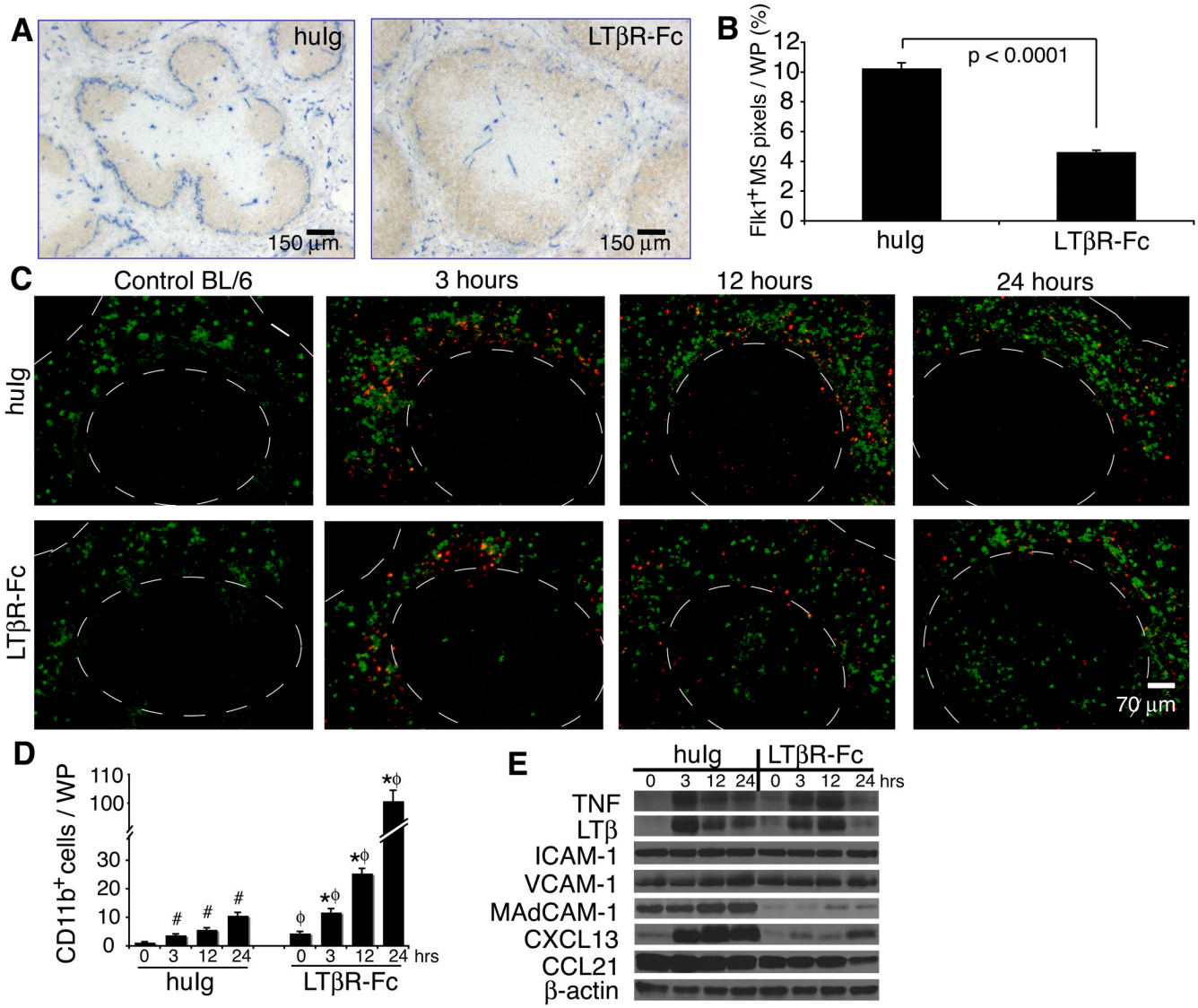

Figure 6. Intact marginal sinus organization in adult mice is LT-dependent and supports the localization of immune cells within the spleen following challenge by bacterial antigens

(A) C57BL/6 adult mice were treated i.p. with either human IgG1 (huIg) or LTβR-Fc and spleens were harvested 2 wks later. 10 µm sections were stained with anti-Flk-1 (blue) and anti-B220 (brown). Similar results were obtained in 4 additional experiments. (B) The percentage of Flk-1$^+$ MS structures per WP area was quantified from 10 µm sections using a 20× objective (n≥40 WP nodules from 3 independent experiments; graph shows mean + S.D.). (C) C57BL/6 mice were treated i.p. with either huIg or LTβR-Fc and 2 wks later were injected i.v. with 250 µg of TMR-labeled *S. aureus* bioparticles (red). Spleens were harvested at 3, 12 or 24 hrs after injection with the particles and sections were stained with anti-CD11b (green). Dashed lines outline WP areas. (D) The numbers of CD11b$^+$ cells localized in the WP was quantified from ≥40 WP areas from 3 independent experiments with 3–5 mice per group. Graph shows mean + S.D. (E) Expression levels of the indicated cytokines, chemokines and adhesion molecules were analyzed by immunoblotting. Data are representative of at least 3 independent experiments with 3–5 mice per group.